Computer Communications 164 (2020) 215–228

Contents lists available at ScienceDirect

Computer Communications

journal homepage: www.elsevier.com/locate/comcom

Joint link-level and network-level reconfiguration for urban mmWave wireless backhaul networks

Yuchen Liu *, Qiang Hu, Douglas M. Blough

Georgia Institute of Technology, Atlanta, USA

ARTICLE INFO

Keywords:
Millimeter wave
Wireless backhaul
Relay nodes
Survivability
Reconfiguration
Robustness
Blockages

ABSTRACT

Due to the rapid densification of small cells in 5G and beyond cellular networks, deploying wired high-bandwidth connections to every small cell base station (BS) is difficult, particularly in older metropolitan areas where infrastructure for fiber deployment is lacking. For this reason, mmWave wireless backhaul has been proposed as a cost-effective and flexible alternative that has the potential to support the high data rates needed to accommodate backhaul traffic demands. To address the robustness of such networks, we investigate a novel relay-assisted backhaul architecture, where a number of small-cell BSs and relays are deployed, e.g. on the lampposts of urban streets. In this scenario, the interconnected logical links constitute a mesh network, which offers opportunities for both link-level and network-level reconfiguration to overcome blockages and/or node failures. We present two joint link-network level reconfiguration schemes for recovery after exceptional events. One prioritizes relay path (link-level) reconfiguration and uses alternate network-level paths only if necessary. The other splits traffic on both reconfigured logical links and backup network paths to improve throughput. Through simulation, the reconfiguration schemes are shown to not only provide near-optimal backhaul survivability but to also maintain high network throughput across a range of scenarios for urban mmWave backhaul networks. The schemes are also validated to significantly outperform existing purely link-level and purely network-level reconfiguration schemes.

1. Introduction

5G and beyond cellular networks are rapidly being deployed to meet ever-increasing mobile traffic demands. Dense deployment of small-cell base stations (SBSs) in these networks is a key feature that will increase network capacity and maintain coverage [1]. In dense small-cell networks, it is widely recognized that deploying fiber connections to every SBS for backhaul is cost-prohibitive and, in many locations, infeasible [2,3]. Due to the very high achievable data rates of millimeter wave (mmWave) communication, mmWave backhaul networks are a promising and cost-effective alternative to meet the tremendous backhaul traffic demand [3–9]. However, in order to realize mmWave wireless backhaul in urban environments, the poor propagation and weak penetration characteristics of mmWave communications must be overcome.

Severe penetration loss makes blockage effects a serious problem in mmWave networks [10–13]. Studies have shown that signal strength is degraded by about 20–30 dB when mmWave links are blocked by human beings [14] and obstacles such as buildings and vehicles will effectively completely block mmWave signals. Therefore, line-of-sight (LoS) conditions are highly desirable to achieve the very high data rates necessary for backhaul traffic. To maintain LoS paths when blockages occur, two approaches are: (1) adopting a network topology with redundant communication paths that offer opportunities for network-level reconfiguration, and (2) developing effective path reconfiguration mechanisms, which can be applied to quickly recover from exceptional events such as blockages and failures.

With respect to network topologies for mmWave wireless backhaul, there are primarily two architectures: centralized and distributed [6]. In a centralized architecture, a macrocell BS (M-BS) is situated in the center with a number of SBSs connected to it via direct links, which form a star topology. With a star topology, it is not possible to recover from link failures since there is only one route from each SBS to the M-BS. However, in a distributed architecture, SBSs form a mesh-like backhaul network, where traffic is relayed on SBS to SBS links to/from an anchor base station (A-BS), which has a fiber connection to the core network. The distributed architecture is more reliable than the centralized solution, because multiple paths between any SBS and its associated A-BS typically exist. In this architecture, when the communication of a path is blocked, the data can be transmitted to other

* Corresponding author.
E-mail addresses: yuchen.liu@gatech.edu (Y. Liu), qianghu@gatech.edu (Q. Hu), doug.blough@ece.gatech.edu (D.M. Blough).

https://doi.org/10.1016/j.comcom.2020.10.010
Received 30 March 2020; Received in revised form 24 June 2020; Accepted 13 October 2020
Available online 2 November 2020

Fig. 1. Relay-assisted mmWave backhaul network in a section of Manhattan.

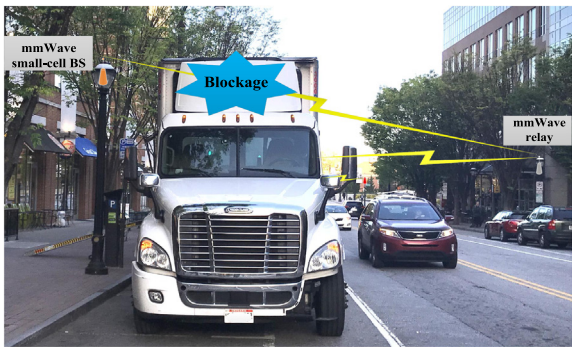

Fig. 2. A parked truck next to a lamppost in an urban environment.

adjacent SBSs and routed on an alternate path to maintain network connectivity.

To achieve a robust mmWave wireless backhaul with high network survivability, our work herein considers a distributed mmWave backhaul network architecture with relay nodes in urban environments. Fig. 1 shows an example of this architecture, deployed in a section of New York City. In this architecture, a number of SBSs and mmWave dedicated relays (shown with green triangles) are deployed along urban streets, which naturally produces a mesh network structure. The deployment of relays between each SBS pair provides multi-hop LoS relay paths between SBSs, which we refer to as logical links in the mesh network. Note that such street-level deployment making use of lampposts has been suggested as a good choice in the 5G era [15–18], because it provides easy access to power, good access tier coverage for users and facilities, and ease of deployment in urban environments. One large project referred to as Terragraph [18] has implemented this network deployment in several cities, such as in Alameda, California and Mikebuda, Hungary. However, these network deployments are susceptible to node failures[1] and/or obstacles in the form of large trucks or other objects that could block some of the primary LoS paths in the network (as shown in Fig. 2). An advantage of our relay-assisted backhaul architecture is that the use of multi-hop logical links allows for link-level reconfiguration when an obstacle blocks an individual physical link. Additionally, the mesh-like network topology makes it possible to use alternate routes for blockage avoidance through network-level reconfiguration. Thus, our network architecture provides opportunities for both link-level and network-level reconfiguration, which can be combined to produce a network with very high survivability in the presence of obstacles and/or node failures.

Based on this backhaul network architecture, we present two joint link-network level reconfiguration schemes to tolerate blockages and/or node failures. The main contributions of this work are as follows:

(1) We introduce a novel relay-assisted mmWave backhaul network architecture for 5G and beyond cellular networks in urban environments, which offers opportunities for both link-level and network-level reconfiguration to overcome potential blockages/failures.
(2) We specify the first joint link-network level reconfiguration approach to address the backhaul survivability problem, where relay path (link-level) reconfiguration is prioritized and alternate network-level paths are used only if necessary.
(3) To minimize the overhead when network-level reconfiguration is necessary, we formulate and efficiently solve two knapsack-like problems to decide which SBSs will be moved to alternate paths. Our first method yields a solution that minimizes the number of SBSs that have to be reconfigured, while our second method minimizes the number of paths that need to be reconfigured.
(4) To further improve throughput performance with blockages in the network that support multi-path routing, we present another novel reconfiguration approach to use primary and backup paths in combination, and we derive the optimal split of data traffic over the multiple selected paths.
(5) Through extensive simulations, we evaluate network performance of our proposed schemes and show that they significantly outperform existing reconfiguration approaches in multiple dimensions such as network survivability, throughput, and latency performance. In particular, the network robustness provided by the proposed schemes is shown to be near-optimal, i.e. it is very close to an upper bound that we derive on network survivability.

The remainder of the paper is organized as follows. Section 2 discusses related work. In Section 3, we introduce our relay-assisted mmWave backhaul network architecture. Section 4 analyzes secondary interference and NLoS paths in the considered network architecture. In Section 5, we present our joint link-level and network-level reconfiguration schemes to overcome blockage effects. Network performance under different conditions is quantified through simulation in Section 6, and Section 7 concludes.

2. Related work

In this section, we review the prior works on mmWave wireless backhaul and reconfiguration approaches to overcome blockages.

2.1. Design of mmWave backhaul networks

Among related works on mmWave wireless backhaul networks, some advocate an in-band solution [19–23] where access and backhaul tiers occupy the same frequency band, while others consider an out-of-band approach, such as in [5,15,24,25], where the two tiers each have their own distinct (non-overlapping) frequency band. The latter approach can utilize extra frequency bands for backhaul, and the decoupling of the two tiers simplifies the system design, as there is no cross-tier interference.

Most wireless backhaul architectures that have been proposed are of the self-backhaul type [19,26–29], where SBSs directly connect to each other, and SBSs themselves serve as relay nodes to form multi-hop routes in the backhaul network. However, a self-backhaul architecture can be difficult to achieve in urban environments due to the abundant obstacles that occur there, which can block LoS paths between neighboring SBSs. To address this issue, some works have

[1] The node-failure case is equivalent to a blockage case where an obstacle totally blocks the node. Thus, in the remainder of the paper, we mainly focus on blockage effects.

proposed dedicated mmWave relay devices deployed in the backhaul network in between SBSs so that all physical links operate on LoS paths [5,15,17,30]. In [15], the authors proposed a multi-hop mmWave backhaul in the street canyon scenario, but the orthogonal frequency based schedule limits the scale of the linear backhaul network, which results in a lower throughput. To tackle this problem, the authors of [5,17,30] studied the optimal scheduling and topology construction in relay-assisted mmWave backhaul networks, where the throughput of a single logical backhaul link can achieve over 10 Gbps under LoS conditions [17].

In addition, recent advances in improving throughput of LoS mmWave links can be used in conjunction with relays to improve backhaul network performance. Techniques such as mmWave LoS MIMO [31,32] and mmWave orbital angular momentum [33] fall into this category. These approaches would be particularly beneficial for the links near the A-BS (see Fig. 1) since they have the highest traffic demands in the entire backhaul network.

2.2. Survivability of wireless multihop networks

Prior work on survivability of multihop wireless networks can be broadly categorized into two main approaches: network-level reconfiguration (NLR) and link-level reconfiguration (LLR).

2.2.1. Network-level reconfiguration

Network-level reconfiguration schemes mainly use the protection method or the restoration method. The protection method reserves backup resources before link failure occurs, whereas the restoration method finds a new path for the affected traffic after a failure. Specifically, [34,35] proposed analytical methods and path restoration schemes to prevent single-link failures in wavelength-division-multiplexing optical networks. While in wireless multi-hop networks, most related works focus on the protection method, because it can achieve fast recovery [36–39]. In [36], the author developed an effective heuristic algorithm to find disjoint backup paths in survivable networks, which shows the good performance on both optimality and running time. In [37], a dynamic routing algorithm to select the minimum-cost backup path was proposed, which improves utilization and reduces blocking in mesh networks. In [38], another method was introduced that pre-computes a set of backup paths for each active path, and uses the multiple survivable paths between each pair of nodes to survive any single risk. In [39], the author proposed a lossy probabilistic network model with obstacle shadow awareness ability, which is used to find multiple lossy paths for path recovery.

In between the protection method and restoration method, there also exist several works that adopt a predictive method for network reconfiguration [40–42]. The main idea in these approaches is to find and reconfigure the backup path in advance if the link failure is predicted to occur. For example, [40] proposed a multi-hop heuristic path-reconfiguration algorithm to prevent the early death of sensor nodes based on the prediction of energy consumption, which improves the overall network life time in wireless sensor networks. In the context of mmWave networks, [41] analyzed the impact of weather on link reliability, and presented a predictive weather-assisted routing protocol that routes data around potential link failures. In [42], a learning-based approach was proposed to predict if a primary mmWave link would experience blockage, and the serving BS uses this information to proactively hand over the user to a backup BS with a LoS link.

One issue with network-level reconfiguration for mmWave backhaul is that backup paths might not always exist, because sometimes it is hard to find a candidate path that satisfies both rate and path length requirements.

2.2.2. Link-level reconfiguration schemes

Another approach to blockage handling is based on link-level reconfiguration (LLR), which aims to reconfigure a new relay path within a single logical link between two wireless nodes when a physical link failure occurs. To our knowledge, only a few works have considered multi-hop relay paths for blockage avoidance in outdoor environments [43,44], and they are primarily concerned with finding a relay path with the highest probability of reaching the BS. In contrast, our work considers the maintenance of backhaul paths with very high rates in the presence of temporary blockages. In our previous work [45], the high-throughput path-level reconfiguration algorithm was proposed to reconfigure around temporary blockages in a roadside relay-assisted network topology. In most situations, this scheme maintains high-rate connectivity for logical links between each SBS pair and, in this work, we use it as our comparison point for pure link-level reconfiguration schemes.

Here we note that LLR can be applied in all types of network topologies with relay assistance, and it can be conducted at the SBS level without the participation of the A-BS. However, the link quality will be degraded after reconfiguration since alternative physical links are always longer than the original link and, in general, the link transmission schedule on a reconfigured path is less efficient than the original schedule. In addition, while LLR simplifies network control, it cannot handle some blockage cases, e.g. when the logical link (relay path) is totally blocked.

With our novel relay-assisted mmWave backhaul architecture, this work studies network survivability and presents two joint link-level and network-level reconfiguration schemes. Our preliminary work on this problem demonstrated the basic feasibility of a joint link-level and network-level reconfiguration approach [46]. In this paper, we flesh out this preliminary work by analyzing the interference caused by secondary effects and showing that it is negligible, analyzing the potential use of NLoS paths when blockages occur and demonstrating that they are unlikely to be helpful, providing more detailed reconfiguration algorithms, solving a feasible flow problem that provides a provable upper bound on network survivability, and augmenting the performance evaluation to provide a more complete picture of network performance.

3. Network model

In this section, we introduce the network topology, and channel and antenna models used in the remainder of the paper.

3.1. Network topology in an urban area

For 5G and beyond cellular networks, a large number of small-cell base stations will be deployed in urban areas to cooperatively provide a more reliable access experience for users. A number of works have proposed the use of mmWave wireless backhaul for 5G networks [47–49]. Here we consider a relay-assisted mmWave mesh network architecture for backhaul in urban areas [15,50], where mmWave relay nodes are used to assist in connecting BSs of the wireless mesh network.

Fig. 1 shows an example of our relay-assisted mesh backhaul network architecture. In this architecture, there are: a single A-BS connected with fiber to the core network, a number of SBSs deployed at street corners, and several mmWave relays along the roadside (shown with the green triangles). It is assumed that all three of these entities can communicate in the mmWave band using directional antennas with steerable beams, and they produce a number of interconnected mmWave links to form a wireless mesh network. There are three important communication components in our mmWave backhaul network architecture:

- *Physical link*: An actual link between relay pairs or between a relay and its adjacent BS — the capacity of physical links is determined by Shannon's Theorem.

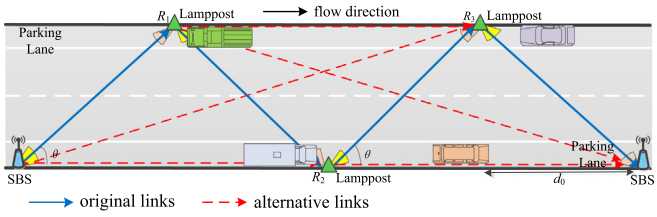

Fig. 3. Original and alternative links in the triangular-wave topology. (For interpretation of the references to color in this figure legend, the reader is referred to the web version of this article.)

- *Logical link (relay path)*: A path between BS pairs including SBS-to-SBS and A-BS-to-SBS, which consists of multiple physical links. The achievable capacity of each logical link is determined by the capacity of its bottleneck physical link pair [5].
- *Backhaul path*: A path between the A-BS and a SBS, which can consist of several logical links. For simplicity, we use $P_{0,i}$ to denote the backhaul path from the A-BS to SBS$_i$.

In this architecture, each logical link between BSs runs along a street and consists of a sequence of mmWave relays. As in [45], we assume that relays are deployed in a regular fashion on both sides of the road, e.g. by deploying them on equally-spaced lampposts. As shown in Fig. 3, these physical links within a given logical link form a triangular-wave topology, where the topology angle θ and horizontal distance between adjacent nodes d_0 are the same everywhere along the topology (as depicted by the blue links of Fig. 3). One advantage of this topology is that the mutual interference along the logical link can be eliminated if θ is made large enough relative to the beamwidth ϕ of the directional antennas.[2] In this way, the logical link can support the 10+ Gbps throughput necessary to meet the requirement for backhaul. On the other hand, this kind of topology is also capable of reconfiguring mmWave links to avoid obstacles (e.g. parked large vehicles) that occur along the roadway. Through adaptive beam steering and dilation when one or more original links are blocked, alternative links can be used to restore the LoS connectivity of a logical link [51]. As an example shown in Fig. 3, when the original link between R_1 and R_2 is blocked, R_1 and R_3 can re-align their directional antennas to create an alternative link for a link-level reconfiguration.

Note that the mmWave relay devices used in the network model are dedicated to a single logical link between a pair of BSs, because we assume relays are simple devices that cannot support the sharing between different logical links. In addition, we assume this kind of simple relay is subject to the primary interference constraint, which means a single relay cannot transmit and receive simultaneously. However, we assume that BSs (A-BS or SBSs) are not affected by these constraints since they are more complex devices with capability to use better antenna isolation and interference cancellation technologies.

3.2. Channel and antenna model

Here we make the standard assumption of additive white Gaussian noise channels. The rate of the directional unblocked physical link p follows Shannon's Theorem with an upper limit, i.e.,

$$R_p \le \beta \cdot B \cdot \log_2(1 + \min\{\frac{P_r(d)}{N_T}, T_{\max}\}) \quad (1)$$

where B is channel bandwidth, N_T is the power of thermal noise, T_{max} is the upper bound of operating signal-noise ratio due to the limiting factors like linearity in the radio frequency front-end, and the link utility ratio $\beta \in (0, 1)$. Considering the primary interference of our simplified relays, $\beta \le 0.5$, and a maximum end-to-end throughput of nearly 16 Gbps can theoretically be achieved in mmWave communications [5]. Here $P_r(d)$ is the received power of the intended transmitter's signal, and equals $k_0 P_t G_t G_r d^{-\alpha}$, where $k_0 \propto (\lambda_w/4\pi)^2$, λ_w is the signal's wavelength, d is the propagation distance, α is the path-loss exponent, and G_t and G_r are antenna gains at the transmitter and receiver, respectively.

In this work, a narrow-beam directional antenna model is adopted for each wireless node, which means that transceiver antennas have a high constant gain G_h within the beam, and a much lower gain G_l outside the narrow beamwidth ϕ. For example, with a 61 element uniform hexagonal array antenna simulated in MATLAB, the antenna gains G_h and G_l are 23.18 dBi and at most 2 dBi, respectively, when the antenna beamwidth is 15°. In Section 4, we do an evaluation of side-lobe effects in our architecture that justifies the statement that mutual interference is eliminated in a properly-constructed triangular-wave topology.

4. Analysis of secondary effects and NLoS paths

To achieve high survivability of mmWave wireless backhaul networks, this work focuses on network reconfiguration with alternative LoS paths in our considered network architecture, and this section provides detailed analyses to justify our adopted approach and assumptions. We first show that the interference caused by secondary effects has only a very small impact on the network performance with our network architecture, and then we demonstrate that it is unlikely that NLoS paths can be used for recovery when a primary LoS path is blocked. Therefore, in subsequent sections, we ignore secondary interference and we focus on reconfiguring logical links using alternative LoS paths or on using alternative paths at the network level.

4.1. Analysis of secondary effects

In this part, we analyze the secondary effects in our considered roadside network scenario, which includes potential interference due to side-lobe effects and ground, vehicle, or building reflections.

4.1.1. Side lobes and ground/vehicle reflections

Side-lobe effects are the interference caused by the antenna's side-lobe emanations. According to the properties of our network topology with appropriate choice of θ (see Section 3.1), it is easy to prove that all of the normal interference cases fall into the side lobe to side lobe category [17], i.e., the interference signal can only be transmitted and received by the antennas' side lobes of nodes, and thus the amount of interference is quite small. For example, choosing some typical parameter values, i.e. narrow-beam directional antennas with a beamwidth ϕ of 15°, G_h of 23.18 dBi, and G_l of 2 dBi, d_0 = 75 m, and θ = 11.7°, the interference-free condition is satisfied according to Theorem 1 in [17]. With these parameters, the signal-to-interference-plus-noise ratio (SINR) on receiver sides drops from 41.18 dB without side lobe effects to 40.58 dB with side lobe effects, which is a negligible difference. While this analysis applies to the topology prior to reconfiguration, any side-lobe effects that occur after reconfiguration will also have a small impact. For example, considering the worst case where the longer alternative link is reconfigured and side-lobe effects occur at the receiver side, the impact on SINR is only around 0.5 dB with respect to the SINR of 25 dB under the normal situation.

Now, considering the reflection effects caused by the ground or vehicles, the interference cases also fall into the side lobe to side lobe category based on the assumption that the ground or the tops of vehicles are flat,[3] therefore, the impact would be less than the side-lobe effects due to the additional reflection loss, i.e. it is still negligible.

[2] According to Theorem 1 in [17], if $\theta - \arctan(\frac{\tan\theta}{3}) > \frac{\phi}{2}$, mutual interference is eliminated.

[3] Under the situation that the ground or the tops of vehicles are not flat, it is possible that the interference signal would be emanated and/or received by the antenna's main lobes, but such situation is fairly rare especially in urban streets we are considering.

Taking the ground reflection as an example, since the measured ground reflection loss ranges from 4.68 dB to 16.98 dB based on [52,53], the reduction of SINR from ground-reflected interference is evaluated as less than 0.3 dB in our network topology, which is negligible with respect to the SINR of over 40 dB on a typical link. In addition, based on a geometric analysis, ground-reflected interference can occur only if $\phi \geq 2 \cdot \arctan(\frac{2h_n}{d_l})$, where ϕ is the beamwidth of antenna, h_n is the height of deployed node, and d_l is the separation distance between two nodes. Thus, this effect can be entirely eliminated with a small enough antenna beamwidth, which is dependent on the specific topology deployed. For instance, if $h_n = 3.5$ m and $d_l = 76.6$ m, ground-reflected interference will not occur if the antenna beamwidth is narrower than 10.4°.

4.1.2. Building reflection interference effects

Different from the vehicle and ground reflection effects, intuitively, the building reflection effects could be an issue in our network topology, since some buildings along the street can reflect a signal and produce secondary interference that might be emanated and received by antenna's main lobes. However, according to the following analysis, we will validate that this effect also has very small impact on network performance, which can even be eliminated with a simple deployment strategy.

As shown in Fig. 4, considering the scheduling in a relay path, interference from building reflections can only occur with a double reflection with two buildings located at exactly the right spots. Note that we ignore the building-reflection effects on further nodes (e.g. N_{k+4}) due to the longer transmission distances and multiple reflections. Based on common building materials, the evaluation result[4] shows that, even with buildings in the right spots, there is typically only around 3 dB reduction of SINR. In the worst case, with two metal buildings at exactly the right locations, the reflection loss would be smaller and the performance loss caused by the building-reflection effects could be noticeable. Even this worst-case scenario can be eliminated, however, by placing antennas on the two sides of the street at slightly different heights causing building reflections to go to the sky or to the ground (as illustrated in Fig. 5). This deployment approach can completely eliminate building reflection effects and is recommended for areas with a high density of metal buildings.

4.2. Potential use of non-LoS paths

In our approach, we have a strong preference for LoS paths due to the need for very high data rates and the high loss that occurs when mmWave signals reflect off most surfaces. Thus, if a physical link stops working due to failure of one of the nodes making up the link or because of an obstacle blocking the LoS path, our link reconfiguration approach uses adaptive beam steering and dilation to bypass the non-functional link (as illustrated in Fig. 3). Here, we discuss whether non-LoS paths could be useful in link reconfiguration.

Consider the scenario shown in Fig. 6, where a large truck blocks the original LoS link between N_{k-1} and N_k. Our link reconfiguration approach may use the link (N_{k-2}, N_{k+1}) or the link (N_{k-2}, N_k) to bypass the affected link in this situation. The green dashed lines in the figure show two building-reflected non-LoS paths that might be able to maintain the link (N_{k-1}, N_k) without reconfiguring the topology.

First, we note that in the case of node failure (of either N_{k-1} or N_k), the non-LoS paths will not work, while our alternative link reconfiguration approach is still possible. Thus, the non-LoS paths are only a possibility in the case of link blockage but not for node failure. Next, we discuss potential non-LoS path usage for the blockage scenario (as shown in the figure).

When considering the building reflections, we note that these are only available in certain situations. For example, if the truck is large enough and positioned as shown in the figure, it could block the reflected signal paths also. Even if those paths are not also blocked by the obstacle, certain geometric conditions (based on factors such as how far the building is from the two nodes, the spacing of relays in the topology, the beamwidth of nodes' antennas, etc.) have to be met for the paths to exist. Additionally, to maintain the high data rates needed for backhaul traffic, the building surface should have a low reflection loss. In practice, only metal buildings are likely to satisfy this condition. Finally, as mentioned in Section 4.1.2, in order to mitigate interference from building reflections, the heights of antennas on the two sides of the street might be different, which would cause the reflected signals to go to the sky or the ground. With this deployment option, signals along NLoS paths from building reflections will definitely not be received by the intended node.

The above discussion indicates that useful non-LoS paths will not often be available to replace a blocked LoS path. Since there is no guarantee of such availability, and also to handle the node failure case, we focus in the remainder of the paper on our alternative link reconfiguration scheme, which reconfigures the topology while maintaining LoS paths between each pair of consecutive nodes. However, this approach could easily be augmented to include opportunistic use of suitable non-LoS paths should the conditions be right for them to function at a high rate. However, in our simulations, we make the assumption that such conditions are fairly rare and so we do not simulate this augmented approach.

5. Joint link-level and network-level reconfiguration scheme

The ability to reconfigure logical links (relay paths) in the presence of obstacles provides multiple possible approaches to blockage tolerance for the mmWave backhaul network. Link-level blockage tolerance mainly adopts relay path reconfiguration schemes, i.e., finding an alternative LoS physical link to substitute the original blocked link. As for network-level reconfiguration, it usually uses a new high-rate path between the source and destination nodes for blockage avoidance. In this section, we present joint link-network level reconfiguration schemes for fast recovery, which utilize relay path reconfiguration and alternate network-level paths in combination.

5.1. Prioritized link-level reconfiguration

In our considered relay-assisted network scenario, we first propose a prioritized link-level reconfiguration scheme (PLLR), which takes advantage of both link-level and network-level tolerance ability. The main idea is to prioritize relay path reconfiguration to avoid the use of alternate network-level paths whenever possible, so that the A-BS does not need to modify the routing table and inform the SBSs, which might complicate the network control. However, alternative network-level paths can be used if the performance of a reconfigured relay path drops so much that the throughput of that logical link is lower than a threshold value, which means that the original backhaul path $P_{0,i}$ cannot satisfy the data demand at SBS_i. In what follows, we introduce this novel approach in detail.

(1) Backup path selection

To achieve fast recovery, we pre-calculate a set of backup paths for each primary backhaul path and store them in the survivable-path set (SS). Different from other related works that just find one totally disjoint backup path to recover from a single link failure, the SS is used to overcome multiple blockages since obstacles could block a primary path and some of its backup paths simultaneously in our considered scenario. On the other hand, there may not always exist a totally disjoint backup path which also satisfies the high-rate and few-hop constraints, but some partially disjoint paths that meet the requirements can avoid the blockage and could even have better performance than a totally disjoint backup path.

[4] The detailed evaluation results can be found in our companion technical report [54].

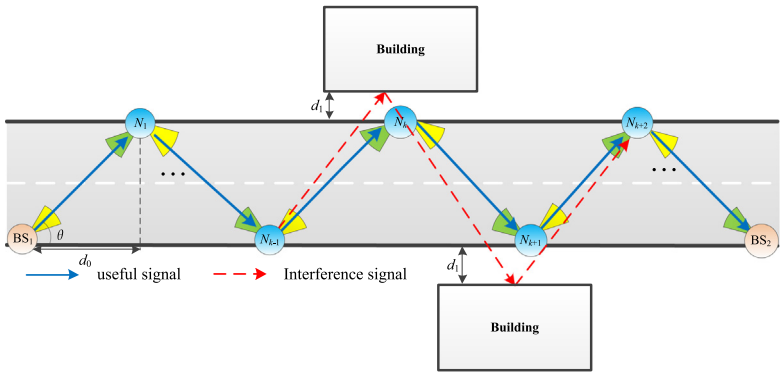

Fig. 4. Building-reflection effects in the network topology.

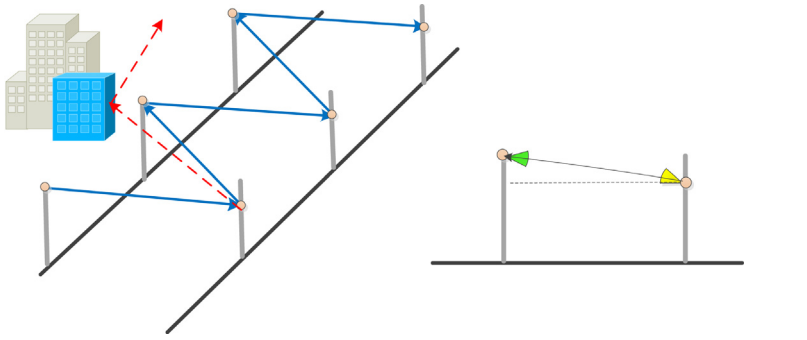

(a) 3-dimentional view of the deployment (b) Front view of nodes on different sides of the street

Fig. 5. The deployment approach to eliminate building-reflection effects.

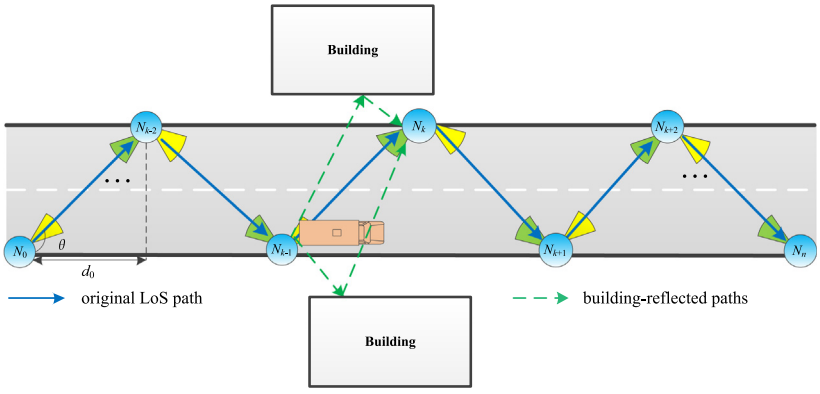

Fig. 6. Possible NLoS paths when blockage occurs.

Fig. 7 shows an example, in which each logical link is characterized by the tuple (hop number, link rate). The original backhaul path $P_{0,8}$ is A-BS→SBS_4 →SBS_5 →SBS_8, and when the logical link between SBS_4 and SBS_5 is blocked, the partially disjoint backup path A-BS→SBS_4 →SBS_7 →SBS_8 has better performance (i.e., with higher rate and fewer hops) than the totally disjoint backup paths (shown with blue lines).

Therefore, our approach finds a SS that consists of a set of backup paths that may not be totally disjoint but can survive blockages, and this enables us to provide protection for a broader range of scenarios and increase the network survivability. Here the backup path selected into SS for potential path recovery should satisfy two requirements: (1) supporting high throughput for mmWave backhaul; (2) with fewer hops than a specified threshold, because too many hops may lead to an unacceptably high end-to-end latency between the A-BS and the associated SBS.

The approach of finding backup paths with higher rates and hop-count constraint is shown in Algorithm 1. Considering the hop counts of different logical links in the topology, we first find the minimum hop count m among these logical links. Then, given a hop-count constraint H (including intermediate relays and relayed-SBSs), we compute a coarse allowable logical-level hops ($maxHop$) as $\lceil H/m \rceil$ (Line 1). After conducting the depth-first search (DFS), we find all backup paths which have their logical-level hop counts $ihop$ no more than $maxHop$ (Line 13–23), and we put each of these paths into the survivable path set $SS[i]$ only if it satisfies the following two conditions: (1) the total hop count of the path is not larger than H (because $maxHop$ used in DFS steps relaxes the real hop-count constraint and some discovered backup paths with more than H hops need to be dropped); and (2) the throughput of the bottleneck logical link pair within the path meets the backhaul rate requirement T (Lines 7–8).

Note that with an appropriate H in most network topologies, there are only a small number of backup paths in each SS. However, we

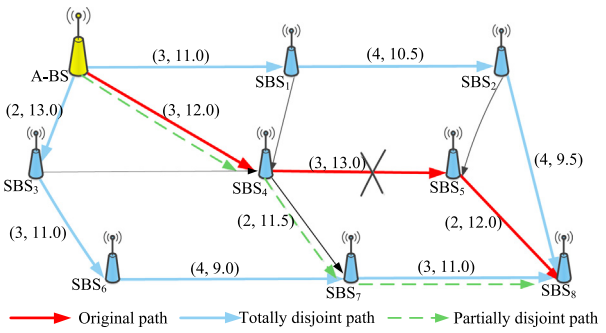

Fig. 7. An example of different backup paths. (For interpretation of the references to color in this figure legend, the reader is referred to the web version of this article.)

Algorithm 1 Finding top-k widest backup paths with hop-count constraint

Input: V, E, H, m, Hop, $thrp$, T
Output: SS

1: $maxHop \leftarrow \lceil H/m \rceil$;
2: **for** each backhaul path $P_{s,i}$ btw A-BS and SBS_i **do**
3: $ihop \leftarrow 0$;
4: $SS[i]$ = searchBackupPath(s, i, V, E, $maxHop$, $ihop$);
5: $SS[i]$.rmv($PrimPath$);
6: **for** each backup path BP_j in SS **do**
7: **if** ($\sum_{l \in BP_j} Hop[l] > H$ || $\min_{l \in BP_j} \{thrp_l\} < T$) **then**
8: $SS[i]$.rmv(BP_j);
9: sort(BP_j, $\min_{l \in BP_j} \{thrp_l\}$);
10: **if** ($SS[i].size > k$) **then**
11: $SS[i]$.rmv($last\ (SS[i].size - k)\ paths$);
12: **return** SS; // get survivable-path sets
Function: searchBackupPath(s, i, V, E, $maxHop$, $ihop$)
13: $path$.add(src);
14: **if** ($i = src$) **then**
15: $SS[i]$.add($path$);
16: $path$.rmv(end node);
17: **return**
18: $id \leftarrow$ find($V.begin, V.end, src$) - $V.begin$;
19: **for** each node j in V **do**
20: **if** (j has been visited) **continue**;
21: **if** ($E[id][j]$! = Inf & $ihop + 1 <= maxHop$) **then**
22: searchBackupPath(j, i, V, E, $maxHop$, $ihop + 1$);
23: $path$.rmv(end node);

also set an upper bound k on the number of backup paths in case the path length constraint is so weak that a large number of possible backup paths exist. In this scenario, we only put the k backup paths with highest rates into SS (Lines 10–12).

The time complexity of Algorithm 1 is $O(N_s^2|E|)$, where N_s is the number of SBSs and E is the number of logical links in the network topology. Note that the algorithm is run at network deployment time, not during network operation, which makes its running time less critical.

(2) Combined link-level and network-level reconfiguration

Algorithm 2 shows the pseudocode for the proposed PLLR scheme, which jointly considers link-level and network-level reconfigurations. In the "Input" arguments, C is a vector that includes the achievable capacity of each logical link between BSs, and NP is a path set that contains each backhaul path $P_{0,k}$ between A-BS and SBS_k in the network. D and AD are the sets that include data-rate demand of each SBSs and the aggregated data-rate demand of each logical link, respectively, and the link much closer to the A-BS will have higher aggregated data-rate demand since it is required to carry more traffic to further SBSs. SS contains the survivable-path set SS_k of each $P_{0,k}$, which is obtained by running Algorithm 1. When the logical link $\mathcal{L}$ between BS_i and BS_j is blocked, the high throughput link-level reconfiguration algorithm (HTPR) is first executed for logical link recovery.

Algorithm 3 explains the HTPR algorithm in detail, and as an example shown in Fig. 3, HTPR executes on node R_1 when the original link between R_1 and R_2 is blocked. After performing the blockage detection process [51] in the topology, different alternative link sets *altPath* are searched based on the four-type blockage model in [45] (Lines 1–2). To achieve higher throughput, shorter alternative physical links, such as the link between SBS and R_2, are given priority in *altPath* (Lines 5–6), but if none of them are available, other longer alternative links can be chosen, such as the link between SBS and R_3. Besides, the larger-index link is preferred, e.g. the link between R_1 and R_3 has priority over the link between SBS and R_2, because it may circumvent other obstacles that take effect on higher-numbered links (e.g. avoiding the possible blockage of the link between R_2 and R_3 as well). When consecutive alternative links need to be selected (e.g. if all original links are blocked), shorter and longer links will be assigned alternated priorities to prevent the topology degenerating to a straight line, which is subject to severe self interference (Lines 7–8). Note that an alternative link can be selected (viewed as *goodPath*) only if its start and end node exist in *Path*, and the end node is not failed (Line 4). After selecting the alternative link *newLink*, the reconfigured logical link $newLogLink$ is produced (lines 9–11), otherwise (i.e., no alternative relay paths can avoid this blockage), this logical link is viewed as a failed link with very low rate due to blockages (Lines 12–14).

Now we move back to Algorithm 2, after running this link-level reconfiguration algorithm, the achievable capacity of this logical link $\mathcal{L}$ will be degraded since one or more longer physical links would be selected for blockage avoidance, and then C is updated with the new capacity of $\mathcal{L}$ (Lines 2–3).

If the current throughput of the degraded link $\mathcal{L}$ drops lower than its aggregated data-rate demand (AD) (Line 3), all SBSs backhauled by the link $\mathcal{L}$ are found and put into $B_{\mathcal{L}}$ (Lines 4–5). Then the network-level reconfiguration will be activated to select alternate backup paths for some of the affected SBSs.

For example, Fig. 8 shows several primary backhaul paths, and every logical link has the achievable capacity of 12 Gbps and data-rate demand at each SBS_i is D_i. From further SBSs to A-BS, we can compute the AD of each logical link in turn (shown in Fig. 8). Now assuming the current capacity of link $\mathcal{L}_0$ (between ABS and SBS_1) drops to $C_{\mathcal{L}_0}$ ($C_{\mathcal{L}_0} < AD_0$), all backhauled SBSs ($SBS_1 \sim SBS_8$) are obtained. In order to avoid the use of more alternate network-level paths which might complicate the network control, we set an objective to minimize the number of SBSs that need to be reconfigured to use backup paths (referred to as rSBSs).

One direct method of minimizing rSBSs (MRS) is to formulate the following optimization problem:

$$\max_{S} \sum_{i \in B_l} s_i \tag{2}$$

$$s.t. \sum_{i \in B_l} D_i \cdot s_i \le C_{\mathcal{L}}, \quad s_i \in \{0, 1\} \tag{3}$$

where s_i is the SBS backhauled by the logical link $\mathcal{L}$. The objective function in Eq. (2) aims to satisfy the greatest number of SBSs affected by this link. Eq. (3) indicates the capacity constraint, where the aggregated data-rate demand on the link $\mathcal{L}$ cannot exceed its current capacity, and s_i will be set as 1 if SBS_i is chosen, otherwise it equals to 0. This optimization problem is similar to the *0/1 knapsack problem*, and in this case the optimal solution is to sort the SBSs in order of increasing data-rate demand and satisfy them in turn until there is not enough capacity

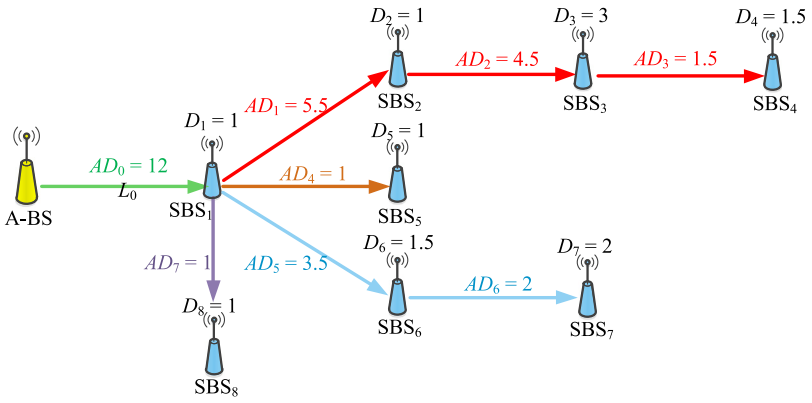

Fig. 8. An example for minimizing rSBSs. (For interpretation of the references to color in this figure legend, the reader is referred to the web version of this article.)

Algorithm 2 Prioritized Link-Level Reconfiguration

Input: C, NP, AD, SS, D
Output: updated NP

1: HTPR($\mathcal{L}$, Relay[i][j]); // link-level reconfiguration
2: C.update($C_{\mathcal{L}}$);
3: **if** ($C_{\mathcal{L}} < AD_{\mathcal{L}}$) **then**
4: **for** each $P_{0,k}$ in NP contains $\mathcal{L}$ **do**
5: $B_{\mathcal{L}}$.add(s_k);
6: $G \leftarrow$ Group(s_k, $P_{0,k}$);
7: sort($g_k \in G$, $AD_k \uparrow$);
8: **for** $k \leftarrow 0$ to size(G) **do**
9: **if** ($AD_k \leq C_{\mathcal{L}}$) **then**
10: G_s.add(s_k); // satisfied groups
11: $C_{\mathcal{L}} \leftarrow C_{\mathcal{L}} - AD_k$;
12: **else break**; // not enough capacity
13: $G_r \leftarrow G \backslash G_s$; // get remaining groups from G
14: solve(Eq.(2), from g_r with max SBSs);
15: **for** each g_r in G_r **do**
16: AltPath(L-SBS$_m$, when max(Th_i) $\geq D(m)$);
17: max(Th_i)$\leftarrow$ max(Th_i) - $D(m)$;
18: **for** each NL-SBS$_k$ with fewer backup path first **do**
19: **if** (HC & DC) = false **then**
20: AltPath(NL-SBS$_k$, when max(Th_j) $\geq D(k)$);
21: **else**
22: max(Th_i) $\leftarrow$ max(Th_i) - $D(k)$;
23: AD.update; NP.update;
24: **return** NP; // get updated network-level paths

of link $\mathcal{L}$ to backhaul any SBSs. As an example, in Fig. 8, when the capacity of the logical link between A-BS and SBS$_1$ (shown with green line) drops to 7 Gbps, we need to reconfigure new backhaul paths for SBS$_3$ and SBS$_7$.

However, this MRS method does not take into account the primary working paths, so we introduce another method to minimize rSBSs with groups (MRG).

In the MRG method, if the current capacity of link $\mathcal{L}$ drops below $AD_{\mathcal{L}}$, we first group all SBSs backhauled by link $\mathcal{L}$ according to their primary paths in set G. As an example, in Fig. 9, when $C_{\mathcal{L}_0} < AD_0$, all backhauled SBSs can be divided into three groups based on their primary paths. After that, we start to minimize the number of groups that cannot be fully satisfied, i.e., maximize the number of satisfiable groups by solving a similar knapsack-like problem:

$$\max_{G} \sum_{g \in G_l} g_i \tag{4}$$

$$s.t. \sum_{i \in G_l} AD_{g_i} \cdot g_i \leq C_{\mathcal{L}}, \quad g_i \in \{0,1\} \tag{5}$$

where each g_i includes the grouped SBSs backhauled by the logical link $\mathcal{L}$, and AD_{g_i} is the aggregated data-rate demand of each group. After obtaining the groups that can be fully satisfied, the remaining items in G are the groups g_r that need to be reconfigured. Starting from the g_r that comprises the maximum number of SBSs, we break g_r and repeat solving the knapsack-like problem in Eq. (2) with the remaining $C_{\mathcal{L}}$, so the minimum number of rSBSs in each group can be obtained.

In this way, for each group g_r that is not fully satisfied, we only need to reconfigure the new backhaul path for the rSBS closest to the degraded link $\mathcal{L}$, i.e., the leader rSBS (L-SBS), because the paths from the L-SBS to other non-leader rSBSs (NL-SBS) can still be maintained within the group. Different from the MRS method that will alternate new backhaul paths for all rSBSs, here we try to force rSBSs in one group and then only take care of the leader rSBS, which can reduce the reconfiguration overhead.

Note that for those NL-SBSs in each group g_r, we also need to check whether or not each of them violates the following two constraints:

- *Hop-count constraint (HC)*: The total hop counts of the new reconfigured path and the maintained path for the NL-SBS should be less than the hop-count threshold H.
- *Data-demand constraint (DC)*: The available capacity of that new reconfigured path should be able to satisfy the data demand of the non-leader SBS.

If either HC or DC is violated, we need to select a backup path for that NL-SBS from its own SS. Note that we check the NL-SBS that has the fewest backup paths first.

The pseudocode shown in Algorithm 2 uses the MRG method for selecting the base stations to be reconfigured.[5] As described above, the reconfigured groups g_r and corresponding rSBSs can be obtained by solving a knapsack-like problem (Lines 6–14). Then, the network-level reconfiguration is activated to select a new network path for the leader SBS in g_r, and we always select the backup path that has the maximum achievable throughput from its SS (Line 16). Here the achievable throughput performance (Th) of each backup path BP_i can be evaluated as follows:

$$Th_i = \min_{\mathcal{L}_j \in BP_i} \{C_{\mathcal{L}_j} - AD_{\mathcal{L}_j}\} \tag{6}$$

[5] To implement the MRS method, the solution to the knapsack problem of Eqs (2) and (3) can be substituted for Lines 6–14 in the pseudocode.

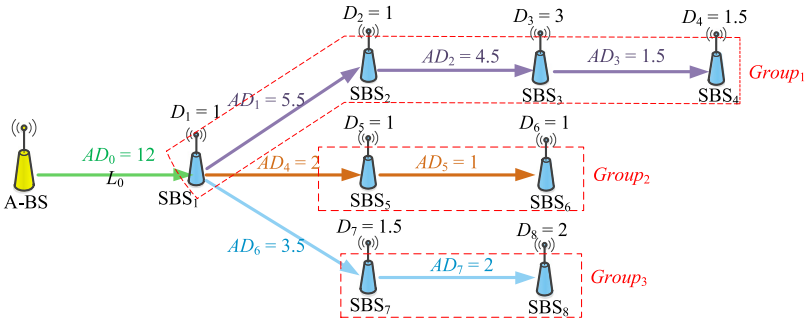

Fig. 9. An example for minimizing rSBSs with groups.

which is determined by the extra available capacity of the bottleneck logical link $\mathcal{L}_j$ within this path. Note that if no backup paths can meet the data-rate demand for this SBS, we have to give up selecting new paths for it. For those NL-SBSs, if either HC or DC is violated, a new path will be selected in the same way (Lines 18–22). In the end, the aggregated data-rate demand set AD and the backhaul path set NP need to be updated (Line 23).

The time complexity of Algorithm 2 can be analyzed as follows. In the worst case, i.e. assuming the degraded $\mathcal{L}$ affects all current backhaul paths such that each of them needs to be reconfigured, Algorithm 2 performs the reconfiguration in time $O(N_s^2)$, where N_s is the number of SBSs. However, the time complexity typically will be much less than $O(N_s^2)$ since we adopt a mesh-like network topology and each degraded logical link will therefore typically only affect a few SBSs. In the best case, if the purely link-level reconfiguration (i.e., Algorithm 3) can save the blocked logical link $\mathcal{L}$ without activating the network-level reconfiguration procedure, the time complexity is reduced to $O(|E|)$, where E is the number of physical links within $\mathcal{L}$.

Algorithm 3 High-throughput link-level reconfiguration

Input: *Path* (includes active nodes), E (includes each physical link $e_{i,j}$)
Output: *newLogLink*

1: $(Blink, BType)$ = BTDProcessFunction(*Path*, E);
2: $altPath$ = FourTypeModel($BType$);
3: **for** *link* in $altPath$ **do**
4: $goodPath$ = testIf($link.src$, $link.dst \in Path$ & $link.dst$ not failed);
5: **if** ($N_k.preNode$ in $Path$! = N_{k-2}) **then**
6: $goodPath$=sortSL($goodPath$); // shorter path first, then larger index first
7: **else**
8: $goodPath$=sortLS($goodPath$); // longer path first, then larger index first
$newLink = goodPath(1)$; // get the first element
9: **if** ($newLink$! = $\emptyset$) **then**
10: Rmv(nodes btw *newLink.src* and *newLink.dst* in *Path*);
11: **return** $newLogLink = Path$;
12: **else**
13: Rmv(all nodes in *Path*); // remove all nodes
14: **return** $newLogLink = \emptyset$; // no substituted relay paths, this logical link is failed

5.2. High-throughput multi-path reconfiguration

To further improve throughput performance with blockages and better leverage the cooperation between the A-BS and SBSs, we introduce another reconfiguration approach based on the previous PLLR algorithm, which is referred to as high-throughput multi-path reconfiguration (HTMR) scheme. This approach uses the primary path and backup paths in combination for data transmission when the blockage occurs, which will work well in networks that support multi-path routing. As a primary relay path's performance is degraded due to link-level reconfiguration around obstacles, some of its traffic can be off-loaded to backup paths so that the reconfigured relay path and several alternative routes are used at the same time. Before adopting this algorithm instead of PLLR, we should pre-evaluate how much performance increase can be achieved compared to the PLLR scheme, since the benefit will depend on the overall network topology and the traffic flows, and HTMR scheme should be used for path recovery in the scenario where it can provide substantial benefits on throughput and is therefore worth the added network control complexity for multi-path transmissions.

First, we need to solve a network flow problem in order to determine how to split traffic among the degraded primary path and backup paths which are totally disjoint. To split the traffic among multiple available paths, assuming there are n possible network paths between A-BS and SBS$_i$ with the data demand D, their respective achievable data rates R_i can be obtained according to Eq. (6). In this way, the required transmission time over each path is $t_i = d_i/R_i$ $(i \in P_s)$, where d_i is the traffic assigned on path i. Assuming the data d_i over each path is transmitted from A-BS to SBS$_i$ at the same time, we can get the total required time T_r until all data D has been received as follow:

$$T_r = \max\{\frac{d_1}{R_1}, \frac{d_2}{R_2}, \ldots, \frac{d_n}{R_n}\} \tag{7}$$

Thus the end-to-end throughput can be obtained as D/T_r. To maximize the throughput performance by splitting traffic over multiple paths, we formulate the optimization problem as follows:

$$\max_{\{d_i\}_{i\in P_s}} D \cdot \min\{\frac{R_1}{d_1}, \frac{R_2}{d_2}, \ldots, \frac{R_n}{d_n}\} \quad s.t. \sum_{i\in P_s} d_i = D, R_i \geq 0, d_i \geq 0. \tag{8}$$

Theorem 1. *To maximize the end-to-end throughput with given data demand D between A-BS and SBSs along n possible routes, the assigned traffic for each route should be proportional to its achievable rate, i.e.,*

$$d_i = \frac{D \cdot R_i}{\sum_{i\in P_s} R_i} \ (1 \leq i \leq n). \tag{9}$$

Proof. The objective function in Eq. (8) can be rewritten as max $D\tau$, $R_i/d_i \leq \tau \ \forall i$. By making each R_i/d_i be equal, the Karush-Kuhn–Tucker condition will be satisfied and we can get the optimal solution as $\sum_{i\in P_s} R_i$. Therefore, the optimal value d_i is obtained as

$DR_i/\sum_{i\in P_s} R_i$, which is proportional to R_i. If each R_i/d_i is not split equally, e.g., $R_j/d_j > \sum_{i\in P_s} R_i/D$, which means that $d_j = (D \cdot R_j/\sum_{i\in P_s} R_i) - \epsilon$, and this would result in another split data $d_k = (D \cdot R_i/\sum_{i\in P_s} R_i) + \epsilon$ since the total demand should be unchanged. Therefore, R_k/d_k becomes the bottleneck value and will reduce the original optimal solution. □

As an extension of the PLLR scheme, the basic logic of HTMR algorithm is similar to Algorithm 2, but the main difference is the method to select network-level paths for each rSBS (L-SBS or NL-SBS), which is shown in Algorithm 4. First, if the degraded logical link $\mathcal{L}$'s capacity is not used up (Line 2), both the primary path $P_{0,k}$ and backup paths can be possibly used for rSBS, otherwise only backup paths will be used for reconfiguration. In both of these cases, we first need to find the disjoint backup paths in SS (Line 4). Here, an approach referred to as *joint-weight selection* is designed to obtain the maximum number of disjoint backup paths in SS (shown in Eq. (10)), where each selected path p_i does not have any overlapping logical links $\mathcal{L}$ with other paths.

$$\max_{P} \sum_{i\in SS} p_i \quad s.t. \mathcal{L}_{p_i} \cap \mathcal{L}_{p_j} = \emptyset,\ i \neq j,\ p_{i,j} = \{0,1\} \tag{10}$$

In the case where the primary path $P_{0,k}$ can still be used, we need to put $P_{0,k}$ in SS since it can also be viewed as one of backup paths (Line 3). Then, we start to find disjoint paths in SS_k (Lines 14–22). First, the joint weight W for each backup path BP_i is calculated, which represents the number of paths overlapping with BP_i in SS_k, and these joint paths are recorded in P (Lines 17–19). After that, we select the backup path BP_m with minimum weight W and put it into MP (Lines 20–21). Note that if there exist multiple paths with the same minimum W, the one which has higher throughput will be selected. Finally, we can obtain the maximum number of disjoint backup paths of $P_{0,k}$ until SS_k is empty (Line 15). In the situation where the primary path cannot be used (i.e., $C_{\mathcal{L}} = 0$), we can find maximum number of disjoint backup paths in SS_k without $P_{0,k}$ in the same way.

After obtaining the multi-path set MP, the available backup paths are sorted in order of decreasing rate (Line 5), and the paths with highest rates will be iteratively selected until the data demand D_k at rSBS_k is satisfied (Lines 7–10). In the end, we split the data demand D_k according to Theorem 1, and assign the traffic to each selected path in MP' (Line 12).

The time complexity of Algorithm 4 is $O(k^2 N_s)$, where k is the maximum number of backup paths for each SBS, and N_s is the number of SBSs. Since k is always set as a small value in Algorithm 1, and N_s is usually around 20 or less in an urban area of 1.2 km^2, the algorithm runs extremely fast in areas of that size, which is a typical scenario.

5.3. Upper bound of network survivability

Here, we introduce an approach to evaluate the upper bound of network survivability in the considered network model, which represents the best performance that could be provided by any reconfiguration algorithm. Given a backhaul network N, a reconfiguration algorithm A, and some changes in the condition of the network, we say that the backhaul network N survives if Algorithm A makes all backhaul paths remain connected and they satisfy the data demand of each node with the given network conditions.

Our reconfiguration algorithms described in this section try to keep certain parts of the network unchanged and reconfigure only a subset of the network, which is consistent with practical constraints. However, an algorithm to produce the best possible survivability of a network would consider all possible new network configurations without constraining how much reconfiguration they require. Although this approach is not practical, evaluating such an algorithm can give us an upper bound on network survivability that we can use to see how our algorithms compare to the best possible result.

Algorithm 4 Alternating Multiple Paths for Reconfiguration

Input: C, NP, AD, SS, D
Output: MP'

```
1:  for each rSBS_k do
2:    if (C_L ≠ 0) then
3:      SS_k.add(P_{0,k});
4:    MP = FindDjPath(SS_k);
5:    MP.sort(BP_i, R_i ↓);
6:    R_t ← 0; // init R_t
7:    for i ← 1 to size(MP) do
8:      MP'.add(MP[i]); // add the higher-rate path
9:      R_t ← R_t + R_i;
10:     if (R_t ≥ D_k) then break;
11:   if (R_t < D_k) then return ∅; // do not alternate paths
12:   OptimalTS(path ∈ MP'); // follow Theorem 1
13: return MP';
14: Function: FindDjPath(SS_k)
15: while (SS_k ≠ ∅) do
16:   for each backup paths BP_i ∈ SS_k do
17:     if (BP_i ∩ BP_j ≠ ∅, j ≠ i) then
18:       W_i ← W_i + 1;
19:       P[i].add(BP_j); // add BP_j in joint-path set
20:   FindPath(BP_m with min W);
21:   MP.add(BP_m);
22:   SS_k.rmv(BP_m & path ∈ P[m]);
23: return MP;
```

To derive the algorithm that achieves the highest possible survivability, we first define $x_{i,j}$ to be the flow rate between BS_i and BS_j, $C_{i,j}$ to be the current capacity of logical link $L_{i,j}$, D_i to be the data-rate demand at SBS_i, and $s_{i,j}$ to be the link status of $L_{i,j}$, where $s_{i,j}$ is 1 if $L_{i,j}$ is connected, otherwise it is 0. Then, the reconfiguration algorithm with maximum survivability can be obtained by solving a feasible-flow problem (FFP) with the following conditions:

$$0 \le x_{0,j} \le C_{0,j}, \quad j > 0 \tag{11}$$

$$-C_{i,j} \le x_{i,j} \le C_{i,j}, \quad 0 < i < j \le N-1 \tag{12}$$

$$\sum_{k=0}^{i-1} x_{k,i} \cdot s_{k,i} - \sum_{j=i+1}^{N-1} x_{i,j} \cdot s_{i,j} = D_i, \quad 0 < i \le N-1 \tag{13}$$

where Eq. (11) is the source-node constraint since all data flows are generated from A-SBS, Eq. (12) shows the capacity constraints for non-source nodes, and $x_{i,j}$ is positive if the traffic direction is from SBS_i to SBS_j, otherwise it is set as the negative value. Eq. (13) is the data demand constraint for every non-source node, which means that the sum of all incoming flows minus the sum of all outgoing flows should be the data demand consumed at this node. Now assuming that the network supports multi-path routing schemes, when the capacities of several logical links drop a lot due to blockage effects, the network can be reconfigured with the new network conditions if there exists a feasible solution of all defined flow rates in the FFP; otherwise, we cannot make the network survive no matter what reconfiguration algorithm is adopted. The FFP solution will be used in the next section to provide an upper bound on survivability, against which our more practical algorithms can be compared.

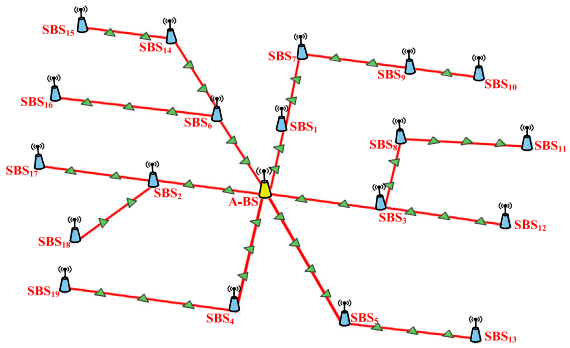

Fig. 10. Primary backhaul paths in the mmWave backhaul network model.

6. Numerical simulations and results

In the face of obstacles that necessitate path recovery in mmWave backhaul networks, we evaluate the network performance including the throughput and blockage tolerance with different reconfiguration schemes. Here we conduct simulations where the mmWave backhaul network is deployed based on the Manhattan urban deployment shown in Fig. 1. With a single centralized A-BS, 19 SBSs at street corners and a number of relays along the roadside are selected. In this scenario, the established logical links between each pair of BSs, which consists of several physical links in a triangular-wave topology, form a mesh-like network that covers the area of over 1.2 km^2.

In Fig. 10, without any link failures, we can compute that the network can support around 3 Gbps data demand for every SBS since each logical link (relay path) can achieve a throughput of around 13 Gbps. Considering potential blockages, we investigate the backhaul network survivability (BNS) and satisfiable data demand for each SBS with our proposed reconfiguration schemes, where BNS is the percentage of cases in which the backhaul network survives out of all simulated cases.[6]

All evaluations are done at the mmWave frequency of 60 GHz with a 2.16 GHz bandwidth. The directional antenna gains G_t, G_r of each wireless node are 23.18 dBi and the transmit power is 1 watt. The attenuation from oxygen absorption is 17 dB/km, and a 15 dB link margin that covers rain attenuation and noise margin is included. Obstacles are generated randomly in the streets and modeled as rectangular vehicles, where their centers fall within the road and form a homogeneous Poisson point process (PPP) of density λ, the widths and lengths are assumed to be i.i.d. distributed and follow the normal distribution $\mathcal{N}(\mu_w = 2.3$ m, $\sigma_w = 0.8)$ and $\mathcal{N}(\mu_l = 8.0$ m, $\sigma_l = 2.5)$, respectively, the orientations are the same as the road's direction, and the heights are assumed to be higher than heights of deployed nodes.

6.1. Network and path survivability

First, we evaluate the performance of the proposed PLLR scheme based on *minimize rSBS method* (MRS) and *minimize rSBS with groups method* (MRG), respectively. The aggregated user demand of each SBS is assumed to be around 1 Gbps, which follows the normal distribution $\mathcal{N}(D_\mu = 1,\ D_\sigma = 0.3)$. On hundreds of simulation runs with random-obstacle scenarios, Fig. 11 shows that MRS and MRG provide very similar BNS across a range of obstacle densities and the achieved BNS is relatively high (above 85% for all but the highest density). However, by adopting MRG method in reconfiguration schemes, the same high BNS can be achieved with fewer reconfigured network-level paths (see

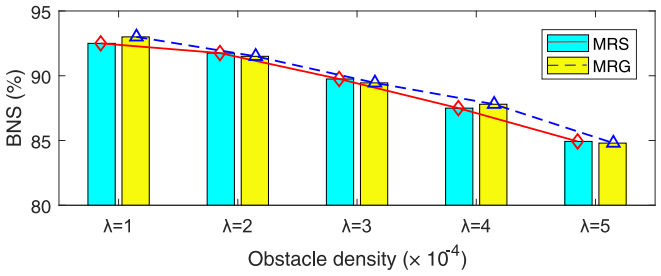

Fig. 11. Survivability comparison between MRS and MRG.

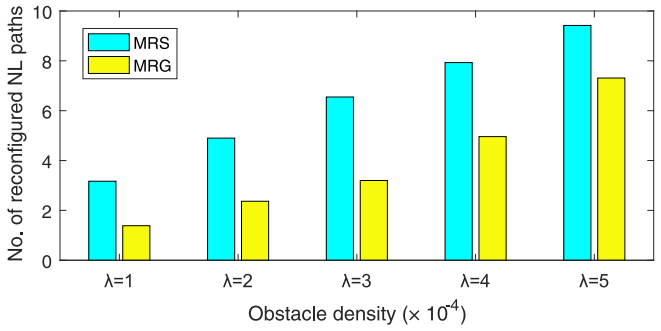

Fig. 12. Number of reconfigured paths comparisons between MRS and MRG.

Fig. 12), especially when the obstacle density is not very high. This is because most of time we only reconfigure a new path for the leader rSBS instead of all rSBSs in the group, which substantially reduces the reconfiguration overhead. Based on this comparison, we adopt the MRG method in both PLLR and HTMR schemes in the remainder of the results of this section.

Second, we show the survivability performance with different reconfiguration schemes. As a comparison, an upper bound of BNS is also reported by solving the feasible-flow problem introduced in Section 5.3. By simulating a large number of random-obstacle cases, Fig. 13(a) shows the survivability performance of different reconfiguration schemes and the upper bound (labeled UB). It is observed that the proposed PLLR and HTMR schemes provide significantly better robustness than purely link-level and purely network-level reconfiguration approaches, where BNS is obviously improved and still over 80% even with a high density of obstacles. Of particular note, the NLR scheme that is adopted by most previous work has worse performance than LLR, and has poor survivability with multiple blockages. On the other hand, we can see that the BNS of our proposed schemes is very close to the upper bound on BNS, and as the obstacle density increases, the performance gaps between the two proposed schemes and the upper bound BNS are 1.2–4.8% and 3.5–8.4%, respectively. Since the PLLR scheme only supports single-path routing and always reconfigures one path for each source–destination pair, the performance gap of PLLR scheme is a little larger than that of HTMR scheme, but it is still around 5% with a not very high obstacle density.

Fig. 14 shows how the BNS of the proposed schemes and the upper bound vary with increasing data demand, for an obstacle density of $\lambda = 2 \cdot 10^{-4}$. As the demand increases, pure network level and pure link level reconfiguration fail to provide survivability in almost all cases. However, our two proposed schemes maintain fairly high BNS and remain close to the upper bound over all simulated demands, which validates that our proposed schemes can provide near-optimal network survivability performance.

To get more fine-grained results, we also evaluate the path survivable rate (PSR), which is defined as the fraction of total backhaul paths that remain connected and satisfy their SBS demand with reconfiguration after blockages occur. Fig. 13(b) shows that PLLR and

[6] Recall that we say the network survives if all backhaul paths remain connected and they satisfy the data demand of each node.

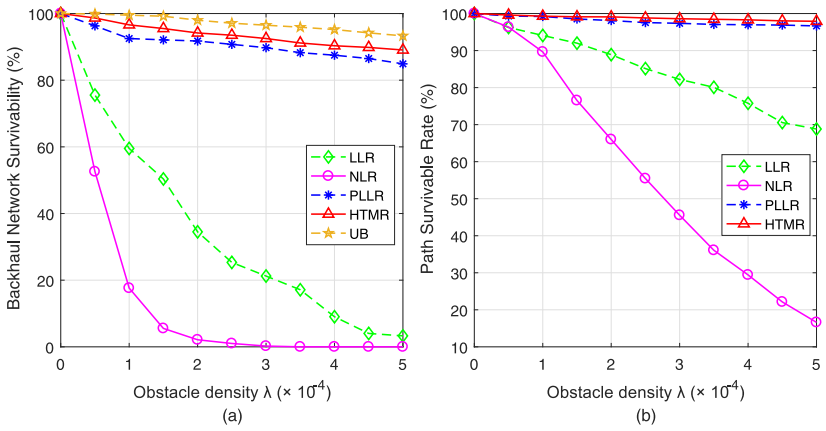

Fig. 13. Network and path survivability comparisons among different schemes.

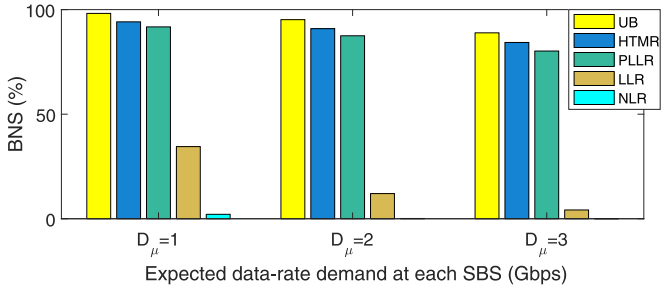

Fig. 14. Network survivability comparisons with different expected data-rate demands.

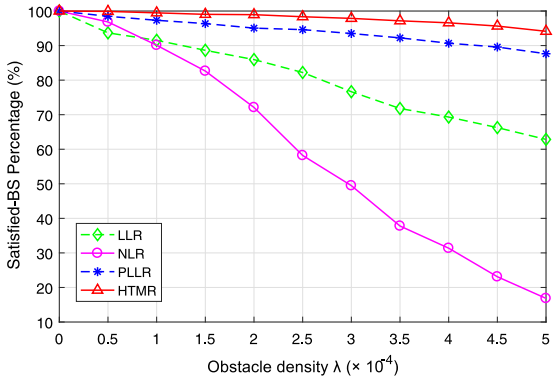

Fig. 15. Satisfied-BS percentage comparisons among different schemes.

HTMR can provide over 97% PSR as the number of obstacles increases, which means that the communication from the A-BS to each SBS would be largely unaffected, even with multiple obstacles. Thus, with the proposed schemes, the blockage tolerance of the entire backhaul network is highly enhanced.

6.2. Throughput performance

In this part, we evaluate whether or not the proposed reconfiguration algorithms can maintain high throughput with blockages, and the satisfied-BS percentage (SBP) is evaluated. SBP indicates the fraction of SBSs that have their respective data demands satisfied. Here, the aggregated user demand of each SBS is assumed to follow the normal distribution $\mathcal{N}(D_\mu = 2, D_\sigma = 0.3)$. From Fig. 15, we can see that HTMR scheme has the best SBP compared with other schemes, since it splits traffic for transmission on both the primary working path and backup paths, which compensates for degraded throughputs on the reconfigured relay paths.

In addition, we vary the data demand D_μ of each SBS and, as expected, the SBP decreases as D_μ increases for both PLLR and HTMR schemes (shown in Fig. 16(a) and (b), respectively). By comparing the SBP based on the same D_μ between these two schemes, we find that the HTMR scheme can satisfy more SBSs than the PLLR scheme with the same obstacle density, and the SBP is improved by more than 20% when $D_\mu = 3$ and the obstacle density is high. Because of such substantial benefits on throughput performance, it might be worth adopting HTMR despite its added complexity.

6.3. Hop-constraint effects

Our problem formulation assumes that each eligible backup path selected for a specific backhaul path should satisfy a hop-number constraint, i.e., the total hops (including dedicated relays and relayed-SBSs) along this path must be fewer than a hop-number threshold H. Here we investigate how this H affects network survivability. With the obstacle density $\lambda = 1.2 \cdot 10^{-4}$ and data demand at each SBS of around 1 Gbps, Fig. 17 shows that the BNS will increase as H increases for all reconfiguration approaches except the LLR scheme. This is because with larger H, more backup paths for each backhaul path are put in the SS, which improves the network-level reconfiguration, but this has no effect on a purely link-level reconfiguration approach. In addition, by increasing H, both PLLR and HTMR can even provide nearly 100% BNS, and NLR can also possibly provide better blockage tolerance than LLR. However, as we show in the next subsection, a larger H can result in higher end-to-end latency and, therefore, this trade-off between latency and robustness in the network would need to be carefully considered with respect to application latency requirements.

6.4. Latency performance

Lastly, we investigate the latency performance of different reconfiguration schemes in our considered scenario. Since the rates of logical links are always high enough to accommodate the data demand of each SBS in our relay-assisted backhaul scenario, and even for reconfigured relay paths with the help of HTPR scheme, the link capacity can still be maintained at over 10 Gbps [45], we ignore queuing delay in this analysis. We, therefore, focus on the end-to-end communication latency, which is equal to the sum of required time slots' durations along the backhaul path of each SBS.

Here we set the packet length to be 5 KB and time slot durations on links at the edge of the topology are then set to be long enough for one packet transmission (e.g., the link between SBS_{17} and SBS_2 in Fig. 10). For links closer to the A-BS, we set longer time slot durations, which are long enough to transmit one packet for each SBS whose traffic flows

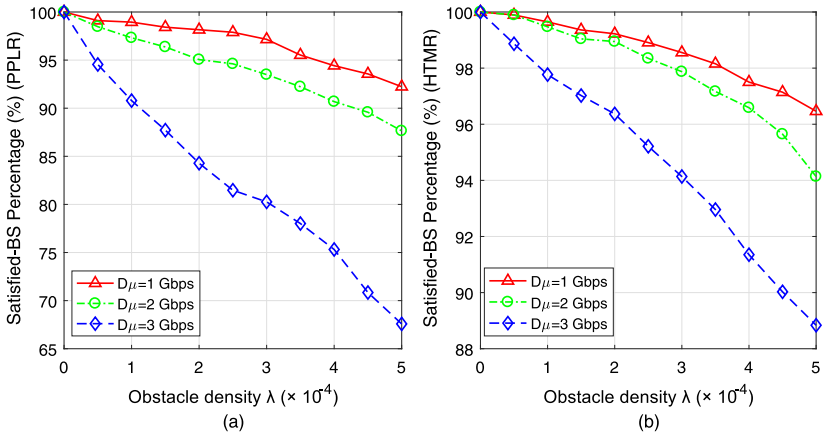

Fig. 16. SBP for PLLR and HTMR with different data demand of SBSs.

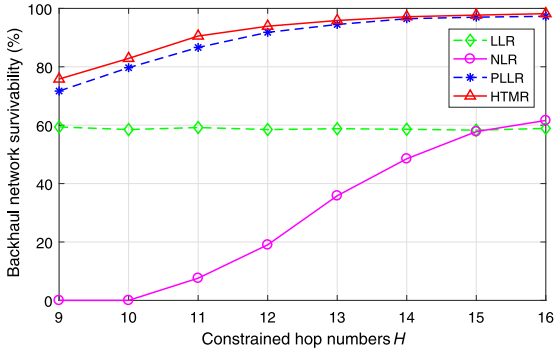

Fig. 17. BNS comparisons with different schemes vs. hop count constraint H.

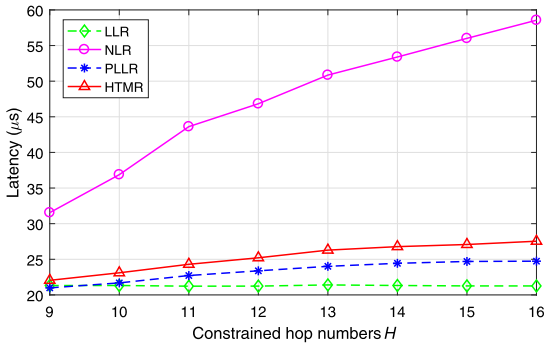

Fig. 18. Average latency for different schemes vs. hop count constraint H.

across the link. This accounts for the aggregate traffic demand that increases for links closer to the A-BS. With obstacle density $\lambda = 1.2{\cdot}10^{-4}$, we evaluated the average end-to-end latency for SBSs vs. the hop-count constraint in the network, and the results with different reconfiguration schemes are reported in Fig. 18.

Fig. 18 shows that, as H increases (meaning more backup paths will be allowed and network survivability will increase), the end-to-end latency increases with most reconfiguration schemes, as is expected. The only exception is the LLR scheme, which is not affected by the hop count constraint since that is only used during network-level reconfiguration. Of particular note, our two joint link-network level reconfiguration schemes show an obvious advantage in latency performance, as compared to the NLR (pure network-level reconfiguration) scheme. In fact, our reconfiguration schemes are not very sensitive to the hop count constraint, especially when H is quite large. This means that, if network robustness is a primary concern, it is advisable to increase H for better network survivability (as shown in Fig. 17) since it has a relatively small impact on the end-to-end latency.

7. Conclusion

In this paper, we studied the survivability of mmWave backhaul networks in urban environments. With a novel relay-assisted backhaul network architecture, where a single A-BS serves as a gateway for a number of SBSs and relays are deployed along urban streets, two joint link-level and network-level reconfiguration schemes to overcome blockage and failure effects were presented. These network reconfiguration approaches combine relay path reconfiguration with alternate backup paths for fast path recovery while minimizing reconfiguration overhead. Through simulation results, the performance of our proposed schemes is shown to be always superior to existing purely link-level and purely network-level reconfiguration schemes. The approaches can provide a substantial improvement in backhaul network survivability, and can also maintain backhaul throughputs, achieving the gigabit-per-second data demand for each SBS even in the presence of multiple blockages/failures.

CRediT authorship contribution statement

Yuchen Liu: Conceptualization, Methodology, Software, Validation, Formal analysis, Data curation, Writing - original draft, Writing - review & editing. **Qiang Hu:** Conceptualization, Validation, Formal analysis, Software. **Douglas M. Blough:** Conceptualization, Methodology, Resources, Formal analysis, Writing - review & editing, Supervision, Project administration, Funding acquisition.

Declaration of competing interest

The authors declare that they have no known competing financial interests or personal relationships that could have appeared to influence the work reported in this paper.

Acknowledgments

This research was supported in part by the National Science Foundation, USA through Award CNS–1813242.

References

[1] C. Wang, F. Haider, X. Gao, et al., Cellular architecture and key technologies for 5G wireless communication networks, IEEE Commun. 52 (2) (2014) 122–130.
[2] M. Coldrey, J.-E. Berg, L. Manholm, C. Larsson, J. Hansryd, Non-line-of-sight small cell backhauling using microwave technology, IEEE Commun. (2013) 78–84.

[3] M. Kulkarni, A. Ghosh, J. Andrews, How many hops can self-backhauled millimeter wave cellular networks support? 2018, arXiv:1805.01040.
[4] F. Wei, Y. Li, D. Jin, L. Su, S. Chen, Millimetre-wave backhaul for 5G networks: Challenges and solutions, Sensors 16 (6) (2016) 892.
[5] Q. Hu, D. Blough, Relay selection and scheduling for millimeter wave backhaul in urban environments, in: Proc. of IEEE International Conference on Mobile Ad-hoc and Sensor Systems, 2017.
[6] X. Ge, H. Cheng, M. Guizani, T. Han, 5G wireless backhaul networks: Challenges and research advances, IEEE Netw. (2014) 6–11.
[7] M. Jaber, F. Lopez-Martinez, M. Imran, et al., Wireless backhaul: Performance modeling and impact on user association for 5G, IEEE Trans. Wireless Commun. 17 (5) (2018) 3095–3110.
[8] B. Sahoo, C. Yao, H. Wei, Millimeter-wave multi-hop wireless backhauling for 5G cellular networks, in: Proc. of IEEE Vehicular Technology Conference, 2017.
[9] X. Ge, L. Pan, S. Tu, et al., Wireless backhaul capacity of 5G ultra-dense cellular networks, in: Proc. of IEEE Vehicular Technology Conference, 2016.
[10] T. Bai, R. Vaze, R. Heath, Analysis of blockage effects on urban cellular networks, IEEE Trans. Wireless Commun. (2014) 5070–5083.
[11] T. Bai, R. Heath, Coverage and rate analysis for millimeter-wave cellular networks, IEEE Trans. Wireless Commun. (2014) 1100–1114.
[12] Y. Liu, D. Blough, Analysis of blockage effects on roadside relay-assisted mmWave backhaul networks, in: Proc. of IEEE International Conference on Communications, 2019.
[13] Y. Liu, Y. Jian, R. Sivakumar, D. Blough, Optimal access point placement for multi-AP mmWave WLANs, in: Proc. of ACM International Conference on Modeling, Analysis and Simulation of Wireless and Mobile Systems, 2019, pp. 35–44.
[14] S. Sur, V. Venkateswaran, X. Zhang, et al., 60 GHz indoor networking through flexible beams: A link-level profiling, in: Proc. of ACM SIGMETRICS International Conference on Measurement and Modeling of Computer Systems, 2015.
[15] J. Du, E. Onaran, et al., Gbps user rates using mmWave relayed backhaul with high gain antennas, IEEE J. Sel. Areas Commun. (2017) 1363–1372.
[16] R. Rony, A. Jain, E. Lopez-Aguilera, E. Garcia-Villegas, I. Demirkol, Joint access-backhaul perspective on mobility management in 5G networks, in: Proc. of IEEE Conference on Standards for Communications and Networking, 2017.
[17] Q. Hu, D. Blough, Optimizing millimeter-wave backhaul networks in roadside environments, in: Proc. of IEEE International Conference on Communications, 2018.
[18] Terragraph: Solving the Urban Bandwidth Challenge, Technical Report, 2019, Facebook Connectivity, https://terragraph.com.
[19] A. Lukowa, V. Venkatasubramanian, Dynamic in-band self-backhauling for 5G systems with inter-cell resource coordination, Int. J. Wirel. Inf. Netw. (2019) 319–330.
[20] R. Taori, A. Sridharan, Point-to-multipoint in-band mmWave backhaul for 5G networks, IEEE Commun. Mag. 53 (1) (2015) 195–201.
[21] M. Polese, M. Giordani, T. Zugno, et al., Integrated access and backhaul in 5G mmWave networks: Potential and challenges, IEEE Commun. Mag. 58 (3) (2020) 62–68.
[22] Y. Li, et al., Integrated access and backhaul optimization for millimeter wave heterogeneous networks, 2019, arXiv preprint arXiv:1901.04959.
[23] A. Rezaabad, H. Beyranvand, J. Salehi, M. Maier, Ultra-dense 5G small cell deployment for fiber and wireless backhaul-aware Infrastructures, IEEE Trans. Veh. Technol. 67 (12) (2018).
[24] Q. Hu, Y. Liu, Y. Yan, D. Blough, End-to-end simulation of mmWave out-of-band backhaul networks in ns-3, in: Proc. of the Workshop on Next-Generation Wireless with ns-3, 2019.
[25] C. Saha, M. Afshang, H.S. Dhillon, Bandwidth partitioning and downlink analysis in millimeter wave integrated access and backhaul for 5G, IEEE Trans. Wirel. Commun. 17 (12) (2018).
[26] T. Vu, et al., Joint path selection and rate allocation framework for 5G self-backhauled mm-Wave networks, IEEE Trans. Wireless Commun. 18 (4) (2019) 2431–2445.
[27] S. Singh, M. Kulkarni, A. Ghosh, J. Andrews, Tractable model for rate in self-backhauled millimeter wave cellular networks, IEEE J. Sel. Areas Commun. 33 (10) (2015) 2196–2211.
[28] A. Ahmed, D. Grace, A dual-hop backhaul network architecture for 5G ultra-small cells using millimeter-wave, in: IEEE International Conference on Ubiquitous Wireless Broadband, 2015.
[29] J. McMenamy, et al., Hop-constrained mmWave backhaul: Maximising the network flow, IEEE Wirel. Commun. Lett. (2019).
[30] Y. Niu, et al., Relay-assisted and QoS aware scheduling to overcome blockage in mmWave backhaul networks, IEEE Trans. Veh. Technol. 68 (2) (2019) 1733–1744.
[31] L. Zhu, S. Wang, J. Zhu, Adaptive beamforming design for millimeter-wave line-of-sight MIMO channel, IEEE Commun. Lett. 23 (11) (2019) 2095–2098.
[32] M. Ivashina, et al., A 1-D steerable beam slotted waveguide antenna employing non-conventional aperiodic array architecture for mmWave line-of-sight MIMO, in: IEEE International Conference on Microwaves, Antennas, Communications and Electronic Systems, 2019.
[33] Y. Ren, et al., Line-of-sight millimeter-wave communications using orbital angular momentum multiplexing combined with conventional spatial multiplexing, IEEE Trans. Wireless Commun. 16 (5) (2017) 3151–3161.
[34] E. Limal, S.L. Danielsen, K.E. Stubkjaer, Capacity utilization in resilient wavelength-routed optical networks using link restoration, in: Proc., Vol. 2, OFC '98, 1998, pp. 297–298.
[35] S. Ramamurthy, L. Sahasrabuddhe, B. Mukherjee, Survivable WDM mesh networks, J. Lightwave Technol. 21 (4) (2003) 870.
[36] D. Xu, Y. Chen, Y. Xiong, C. Qiao, X. He, On finding disjoint paths in single and dual link cost networks, in: Proc. of IEEE International Conference on Computer Communications, 2004.
[37] A. Bigdeli, A. Tizghadam, A. Leon-Garcia, Survivable routing using path criticality, in: Proc. of International Conference on Computing, Networking and Communications, IEEE, 2012, pp. 793–797.
[38] M. Parandehgheibi, H. Lee, E. Modiano, Survivable path sets: A new approach to survivability in multilayer networks, J. Lightwave Technol. 32 (24) (2014) 4139–4150.
[39] T. Wang, L. Leszek, Opportunistic topology control for ad hoc wireless network survivability enhancement based on LIMOS model, J. Netw. Comput. Appl. (2019) 1–12.
[40] M. Asad, M. Aslam, Heuristic path-reconfiguration algorithm using multi-hop opportunistic routing in WSNs, in: IEEE International Conference on Frontiers of Information Technology, 2018.
[41] A. Jabbar, J. Rohrer, V. Frost, et al., Survivable millimeter-wave mesh networks, Comput. Commun. 34 (16) (2011) 1942–1955.
[42] A. Alkhateeb, I. Beltagy, S. Alex, Machine learning for reliable mmWave systems: Blockage prediction and proactive handoff, in: IEEE Global Conference on Signal and Information Processing, 2018.
[43] Y. Niu, C. Gao, Y. Li, L. Su, D. Jin, Exploiting multi-hop relaying to overcome blockage in directional mmWave small cell, J. Commun. Netw. 18 (3) (2016).
[44] S. Biswas, S. Vuppala, J. Xue, T. Ratnarajah, On the performance of relay aided millimeter wave networks, IEEE J. Sel. Top. Sign. Proces. (2016) 576–588.
[45] Y. Liu, Q. Hu, D. Blough, Blockage avoidance in relay paths for roadside mmWave backhaul networks, in: Proc. of IEEE International Symposium on Personal, Indoor, and Mobile Radio Communications, 2018.
[46] Y. Liu, Q. Hu, D. Blough, Joint link-level and network-level reconfiguration for mmWave backhaul survivability in urban environments, in: Proc. of ACM International Conference on Modeling, Analysis and Simulation of Wireless and Mobile Systems, 2019, pp. 143–151.
[47] A. Nasr, Y. Fahmy, Millimeter-wave wireless backhauling for 5G small cells: Scalability of mesh over star topologies, in: Proc. of IEEE International Symosium on a World of Wireless, Mobile and Multimedia Networks, 2017.
[48] Y. Liang, B. Li, M. Yang, et al., MAC protocol framework for 5G mmWave backhaul network, in: Proc. of IEEE International Conference on Signal Processing, Communications and Computing, 2016, pp. 1–6.
[49] R. Taori, A. Sridharan, Point-to-multipoint in-band mmwave backhaul for 5G networks, IEEE Commun. 53 (1) (2015) 195–201.
[50] B. Xie, Z. Zhang, R. Hu, Performance study on relay-assisted millimeter wave cellular networks, in: Proc. of IEEE Vehicular Technology Conference, 2016, pp. 1–5.
[51] Y. Liu, Q. Hu, D. Blough, Blockage type detection process in triangular-wave topology for mmWave wireless backhaul, arXiv:2010.08430.
[52] M. Samimi, T. Rappaport, Characterization of the 28 GHz Millimeter-Wave Dense Urban Channel for Future 5G Mobile Cellular, NYU Wireless Technical Report, 2014.
[53] T. Rappaport, S. Deng, 73 GHz wideband millimeter-wave foliage and ground reflection measurements and models, in: IEEE International Conference on Communication Workshop, 2015.
[54] Y. Liu, D. Blough, Analysis of secondary effects in roadside mmWave backhaul networks, arXiv:2010.10479.